Extended x-ray absorption fine-structure indication of a double-well potential for oxygen vibration in $Ba_{1-x}K_xBiO_3$

2000 J. Phys.: Condens. Matter 12 3767

(http://iopscience.iop.org/0953-8984/12/16/303)

J. Phys.: Condens. Matter **12** (2000) 3767–3786. Printed in the UK PII: S0953-8984(00)07507-X

Extended x-ray absorption fine-structure indication of a double-well potential for oxygen vibration in $Ba_{1-x}K_xBiO_3$

A P Menushenkov and K V Klementev
Moscow State Engineering Physics Institute, 115409 Moscow, Russia

Received 6 September 1999, in final form 16 February 2000

Abstract. X-ray absorption spectra of the oxide systems $Ba_{1-x}K_xBiO_3$ and $BaPbO_3$ above the Bi and Pb L_3 absorption edges were investigated. It was shown that oxygen ions move in a double-well potential and their oscillations are correlated with the charge-carrier movement. The observed breathing-like oxygen vibration in the double-well potential with large amplitude and low frequency causes the strong electron–phonon coupling and high T_c-values for doped $BaBiO_3$. Based on the experimental data, a model of the relationship of the electronic and local crystal structures is proposed that is in good agreement with the results from transport measurements, and inelastic neutron and electron scattering, Raman scattering, and photoemission spectroscopy. In the framework of the model, the possible reasons for the superconductivity in perovskite-like oxides are discussed.

1. Introduction

Although superconductivity was discovered in $BaPb_{1-x}Bi_xO_3$ (BPBO) significantly earlier [1] than in cuprates, the question of the nature of the superconducting state in this oxide as well as in the cognate system $Ba_{1-x}K_xBiO_3$ (BKBO) is still unanswered.

The structures of the crystal lattices of copper oxide high-temperature superconductors (HTSCs) and bismuth-based oxides have some important common characteristics. Both oxide classes have perovskite-like lattices with CuO_n ($n = 4, 5, 6$) or $Bi(Pb)O_6$ complexes joined at the common oxygen ions. In bismuthates, the intersection of octahedral complexes in the three crystallographic directions determines their three-dimensional cubic structure. The CuO_n complexes are joined in CuO_2 planes, which produces the two-dimensional structure of copper oxides.

Because of the strong hybridization of covalent Bi(Pb) 6s, Cu 3d–O $2p_\sigma$ bonds, the above-mentioned complexes are the most tightly bound entities of the perovskite-like structure. Therefore such important peculiarities of perovskite structure as lattice instability with respect to the soft tilting mode of CuO_n or BiO_6 complexes (see for a review [2]) and highly anisotropic thermal factors of oxygen-ion vibration [3], which indicate the large amplitude of rotation oscillations, are inherent to both classes of superconducting oxides and cause anharmonic vibrations of oxygen atoms that may be described as movement in a double-well potential [4,5]. These structural instabilities of the perovskite-like lattice can be related to the transition to a superconducting state [2, 4, 5].

The layered structure of copper oxide compounds, the presence of several non-equivalent copper positions, and there being a number of different Cu–O bonds complicate the local structure analysis. At the same time, the simplicity of the cubic three-dimensional structure

0953-8984/00/163767+20$30.00

of BPBO–BKBO systems makes the interpretation of experimental data easier to a great extent. The relatively low temperatures of the superconducting transition, $T_c \simeq 13$ K for $BaPb_{0.75}Bi_{0.25}O_3$ [1] and $T_c \simeq 30$ K for $Ba_{0.6}K_{0.4}BiO_3$ [6], the values of the superconducting gap, $2\Delta(0)/kT_c = 3.6 \pm 0.1$ for BPBO [7] and $2\Delta(0)/kT_c = 3.5 \pm 0.5$ for BKBO [8], and a sizable oxygen isotope effect [9] allow one to rely on the standard BCS theory of superconductivity, but not excluding a possible realization of other mechanisms. The simpler electronic structure of the s–p valence band of BPBO–BKBO systems in comparison with the d–p band of cuprates favours the establishment of a relationship of the crystal and electronic structures in these compounds.

However, even for these relatively simple systems there has been no agreement so far on a number of crucial aspects: the crystal structure symmetry and lattice dynamics [10, 11]; the electronic structure [12]; the bismuth valence state [13–16]. Most of the unusual properties of $BaBiO_3$-family compounds mentioned in the early review [17] are still unexplained.

In addition, the averaged structural data contradict the local ones. Integral crystallographic methods indicate a simple cubic lattice in BKBO ($x > 0.37$) [11]. In contrast to this, the EXAFS analysis of the four nearest spheres in the bismuth environment [18] reveals a local tilting of octahedra by 4–5°, and Raman spectra provide evidence for a local lowering of the symmetry from simple cubic [19].

An EXAFS analysis of the nearest-oxygen octahedral environment of Bi in the metallic BKBO compound with $x = 0.4$ was previously was made within the harmonic approach [20, 21] and indicated at least one unresolved problem. The temperature dependence of the Debye–Waller factor $\sigma^2(T)$ found by Heald *et al* [20] can be described in the Einstein approximation, which is suitable for harmonic systems, only if one takes into account the temperature-independent factor of 0.0025 Å^2. The attempt to explain this as due to some static disorder with doping was unsuccessful since $\sigma^2(T)$ for the next Bi–Ba and Bi–Bi shells shows the absence of any disorder. Similar weakly varying $\sigma^2(T)$ dependence was found in [21]. Thus, it was observed that the amplitude of the low-temperature Bi–O vibrations in the metallic BKBO compound with $x = 0.4$ is too high (more than twice that for the metallic $BaPbO_3$ compound) [22, 23].

In addition, our careful measurements [23] of temperature-dependent EXAFS spectra of undoped $BaBiO_3$ which were also treated in the harmonic approach showed an entirely abnormal increasing of the σ^2-values for both Bi–O bonds with temperature decreasing from 90 K. We explained these anomalies as showing the influence of anharmonic rotational vibrations of oxygen octahedra which become pronounced at low temperatures [24]; a model connecting superconductivity with rotation-mode asymmetry was proposed [25].

The above contradictions in the description for local structure lead us to the necessity for EXAFS analysis of the nearest Bi–O shell in the anharmonic approach.

In the present paper we report the results of a temperature-dependent EXAFS investigation of BPBO–BKBO systems, treated for the first time by an anharmonic approach based on the idea of such an analysis for apical oxygen atoms in $YBa_2Cu_3O_{7-\delta}$ proposed by Mustre de Leon *et al* [26], We have analysed the EXAFS function $\chi(k)$, using the new program 'VIPER for Windows' [27], by construction of the model potentials of atomic vibrations, subsequent calculation of the pair radial distribution function, and calculation of the model $\chi(k)$. This new approach to the EXAFS analysis of Bi-based oxides gives us an opportunity to investigate the character of oxygen-atom vibrations and, combining the findings with those from our previous local electronic structure studies by XANES (x-ray absorption near-edge-structure) spectroscopy [28], to understand the nature of the structural phase transitions in these systems and to explain practically all the above contradictions.

In section 2 we describe the experimental details and present the procedure of data

treatment. The general results are given in section 3. In section 4 we relate the local crystal structure to the local electronic structure, which is the basis of our processing of the experimental data. In section 5 we discuss the possible superconductive mechanism and demonstrate how the oscillations of oxygen atoms in a double-well potential contribute to superconductivity in BKBO.

2. Experimental procedure and data analysis

In this work we have investigated ceramic samples of $BaPbO_3$ and BKBO with $x = 0, 0.4, 0.5$ synthesized as described in [29]. The materials were examined by x-ray powder diffraction for phase purity. The samples were controlled using transport and susceptibility measurements. $BaBiO_3$ showed semiconductor-like behaviour, and the compositions BKBO with $x = 0.4$ and 0.5 showed typical metallic $\rho(T)$ dependence and superconducting properties with $T_c \simeq 30$ K and $T_c \simeq 16$ K, respectively. The $BaPbO_3$ samples were metallic but not superconducting at all temperatures.

For the XAS measurements, a crushed fine powder was precipitated onto a micropore substrate. The thicknesses of the samples were about two absorption lengths at the chosen absorption edge.

The x-ray absorption spectra were collected at the D-21 line (XAS-13) of the DCI (LURE, Orsay, France) synchrotron operated at the energy 1.85 GeV and the average current ~250 mA of the positron beam at the L_3 edges of Bi (13040.6 eV) and Pb (13426 eV). The energy resolution of the double-crystal Si [311] monochromator (detuned to reject 50% of the incident signal in order to minimize harmonic contamination) with a 0.4 mm slit at 13 keV was about 2–3 eV. The low-temperature measurements were carried out using a liquid-helium circulation-type cryostat with a temperature control of ± 1 K.

The background in the experimental spectra was removed as described in [30], taking care to remove the low-frequency oscillations. The EXAFS functions $\chi(k)k^2$ obtained from the absorption spectra were Fourier transformed in the range of wavenumber k from 1.5 to 16.5 $Å^{-1}$, using the Kaiser–Bessel windowing function. Fourier back-transformation was carried out using a Hanning window from ~1 to ~2 Å corresponding to the first Bi–O near-neighbour shell. In such cases, the number of independent experimental points [31] was $N_{exp} = 2\,\Delta k\,\Delta r/\pi + 2 \approx 11$.

The model EXAFS function for atomic pair absorber–scatterer oscillations is constructed as follows. Suppose we know the potential of these oscillations as a parametric function of interatomic distance. Solving the stationary Schrödinger equation numerically for the particle with the reduced mass of the atomic pair [27], one obtains a pair radial distribution function (PRDF) of atoms in the ith sphere:

$$g_i(r) = N_i \sum_n |\Psi_n(r)|^2 \mathrm{e}^{-E_n/kT} \Big/ \sum_n \mathrm{e}^{-E_n/kT} \tag{1}$$

where N_i is the coordination number, and E_n and Ψ_n are the nth energy level and its corresponding wave function. Given the PRDFs, the model EXAFS function is calculated as

$$\chi(k) = \frac{1}{k} \sum_i F_i(k) \int_{r_{min}}^{r_{max}} g_i(r) \sin[2kr + \phi_i(k)]/r^2 \,\mathrm{d}r \tag{2}$$

where $k = \sqrt{2m_e/\hbar^2(E - E_{th})}$ is the photoelectron wavenumber referenced to the ionization threshold E_{th}, and r_{min} and r_{max} are determined by the windowing function of the Fourier back-transform. The phase shift $\phi_i(k)$ and the scattering amplitude $F_i(k)$ were calculated using the FEFF-6 code [32] for a six-shell cluster with crystallographic data from neutron diffraction

study [11] and using the default set of FEFF-6 parameters. The potential parameters were extracted from the model-to-experimental EXAFS-function fits.

3. General results

In figure 1 (left) we show the experimental EXAFS functions $\chi(k)k^2$ for BKBO with $x = 0$, 0.4, 0.5 and for $BaPbO_3$ measured at the L_3 Bi(Pb) absorption edge at 7 K. The good signal-to-noise ratio seen even for maximal wavenumber values $k \gtrsim 16$ Å^{-1} indicates the high spectral quality. The absence of signal in the Fourier transform in the low-r range of figure 1 (right) testifies to a correct background-removal procedure.

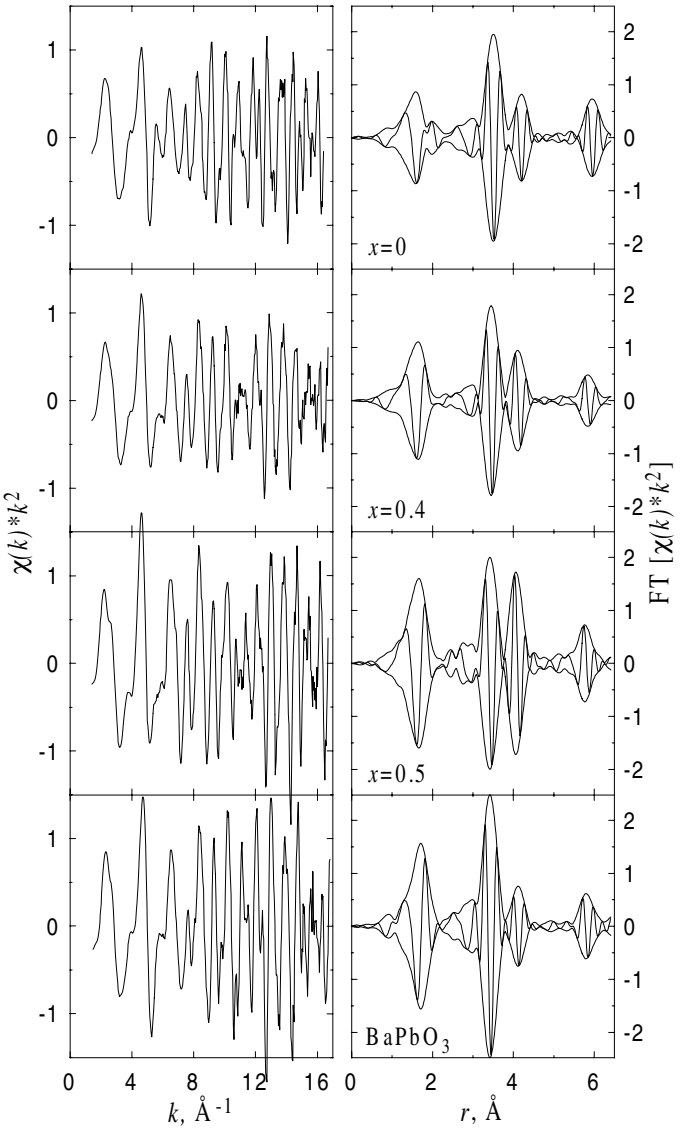

Figure 1. The experimental EXAFS $\chi(k)k^2$ (left) and its Fourier transform magnitude and imaginary part (right) for $Ba_{1-x}K_xBiO_3$ ($x = 0$, 0.4, 0.5) and $BaPbO_3$ at 7 K.

3.1. $BaBiO_3$

EXAFS research [22,33] on $BaBiO_3$ confirms the results of crystallographic works [10,11,13]. According to these, there exist two inequivalent bismuth positions characterized by two Bi–O bond lengths. The equality of the coordination numbers of the two BiO_6 spheres indicates that the $BaBiO_3$ structure represents the ordered alternation of small and large BiO_6 octahedra in the barium lattice. Such an alternation together with static rotation distortion around the [110] axis produce the monoclinic distortion of cubic lattice [10,11,13] (figure 2). As will be shown in section 4, the configuration BiO_6 corresponds to the larger soft octahedra, and $Bi\underline{L}^2O_6$ corresponds to the smaller rigid octahedra. Here, $\underline{L}^2$ denotes the hole pair in the antibonding Bi 6s–O $2p_{\sigma^*}$ orbital of the octahedral complex.

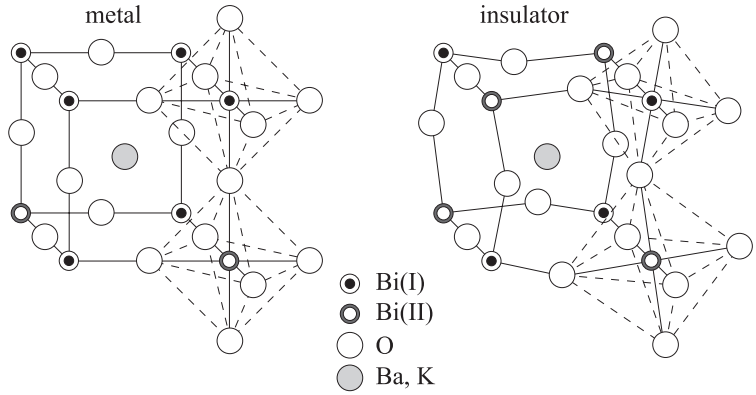

Figure 2. A sketch of the crystal structure of $Ba_{1-x}K_xBiO_3$ in metallic ($x > 0.37$) and insulating ($x < 0.37$) states.

In figure 3(a) the experimental $\chi(k)k^2$ EXAFS for $BaBiO_3$ at 7 K for the first Bi–O near-neighbour shell is shown. The pronounced beating near 8 $Å^{-1}$ is evidence for the existence of at least two different lengths of Bi–O bonds. In all previous EXAFS research [20–23, 33] the EXAFS function was quite successfully fitted in the harmonic approximation as a sum of two independent harmonic functions with different bond lengths and Debye–Waller factors. However, the temperature dependencies of the Debye–Waller factors contradict the harmonic Einstein model [23]. This argues against the independence of oxygen-atom vibrations in two neighbouring octahedra.

In this work, we model the oscillatory Bi–O potential as follows. The inequivalence of the two types of BiO_6 octahedron is due to the presence or absence of a hole pair in the hybridized molecular orbitals Bi 6s–O $2p_{\sigma^*}$ (see section 4). Suppose that the movement of oxygen atoms may transfer a hole pair from one octahedron to another. Such a movement exchanges the roles of two inequivalent octahedra and requires a double-well form of the oscillatory Bi–O potential. Here, we take a parabolic form for each well, $U_1 = \kappa_1(r - r_1)^2/2$ and $U_2 = \kappa_2(r - r_2)^2/2$, and these are joined continuously. Given the calculated $\chi(k)$, defined by equations (1) and (2), we perform a least-squares fit between the model and experimental $\chi(k)$ over the range $k = 2$–16 $Å^{-1}$ (see figure 3(a)). The six parameters determined by the fit were E_{th}, r_1, r_2, κ_1, κ_2, and N. The number of parameters here is the same as for fitting in the harmonic approximation.

The analysis of the parameters of the double-well potential allows one to draw the following conclusions on the oscillations of oxygen atoms in $BaBiO_3$.

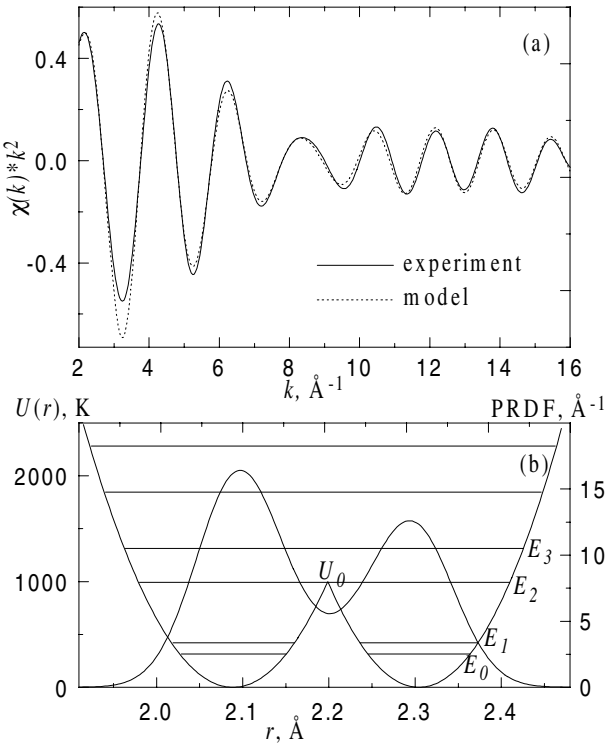

Figure 3. The experimental and model $\chi(k)k^2$ EXAFS for $BaBiO_3$ at 7 K for the first Bi–O near-neighbour shell (a) and the model potential with the corresponding PRDF and energy levels (b). U_0 is the energy of the potential barrier.

(i) At low temperatures there exist two explicit peaks in the PRDF, which is why x-ray and neutron diffraction studies detect the static distortions in $BaBiO_3$.

(ii) Even at low temperatures, the probability of tunnelling between the two wells is non-zero. As will be discussed in section 4, such a tunnelling is equivalent to the dynamic exchange $Bi\underline{L}^2O_6 \leftrightarrow BiO_6$ and explains the observed activation conductivity in $BaBiO_3$.

(iii) The temperature rise leads to a gradual increase of the probability of interwell tunnelling and to the structural transition to the cubic phase found at 750–800 K [13].

(iv) The non-equidistance of energy levels implies that oscillations of breathing or stretching types with several frequencies exist: $\omega_0 = E_1 - E_0$, $\omega_1 = E_2 - E_0$, $\omega_2 = E_3 - E_0$, etc. The latter are gradually manifested at high temperatures.

(v) The positions of the minima of the double-well potential in our model are the *average* positions. They are spaced widely at maximal octahedra tilting and spaced closely at minimal octahedra tilting. In the latter case the probability of interwell tunnelling is maximal. In this sense the tunnelling frequency ω_0 is bounded by a soft-rotation-mode frequency.

3.2. $BaPbO_3$

The experimental $\chi(k)k^2$ EXAFS for $BaPbO_3$ for the first Pb–O near-neighbour shell at all temperatures represents a sinusoid with no beatings and phase breaks (figure 4) and was

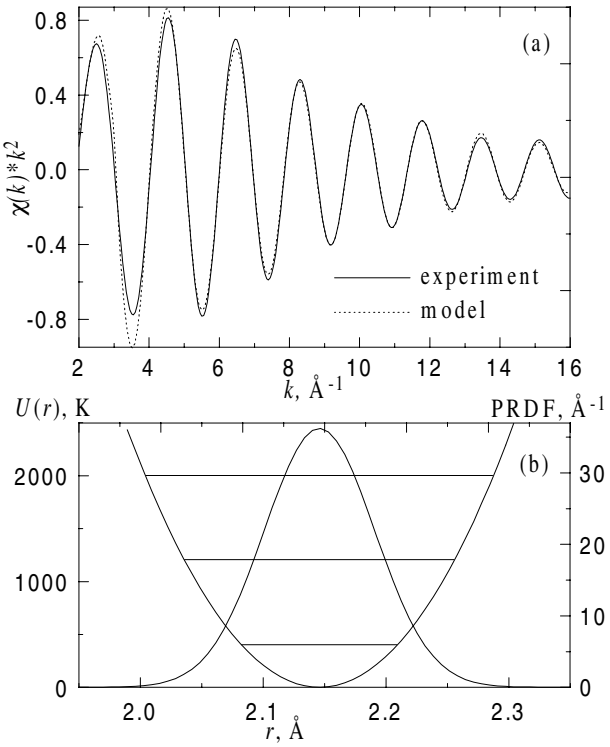

Figure 4. The experimental and model $\chi(k)k^2$ EXAFS for $BaPbO_3$ at 7 K for the first Pb–O near-neighbour shell (a) and the model potential with the corresponding PRDF and energy levels (b).

fitted well using a single-parabolic potential. This means that all Pb–O bonds in $BaPbO_3$ are equivalent and the breathing-type distortion is absent.

3.3. $Ba_{1-x}K_xBiO_3$

The experimental $\chi(k)k^2$ EXAFS function for BKBO ($x = 0.4$) at 7 K for the first Bi–O near-neighbour shell is shown in figure 5(a), by the solid curve. Also, the model calculated in the harmonic approach (as in [20,21]) is shown, as a dash–dot curve. It is seen that in the range $k \gtrsim 12\,\text{Å}^{-1}$ the harmonic approach fails. This argues for anharmonic Bi–O vibration behaviour similar to that in the case of $BaBiO_3$ also occurring in the superconducting compositions of BKBO. A possible tendency in the cubic superconducting materials towards the same type of distortion as in $BaBiO_3$ was pointed out earlier [20, 34].

The K doping of $BaBiO_3$ leads to partial replacement of the larger soft octahedra BiO_6 by the smaller rigid octahedra $Bi\underline{L}^2O_6$ (see the details in section 4). This causes a decrease and disappearance of the static breathing and tilting distortions, but keeps the different rigidities of Bi–O bonds. Hence, the movement of an oxygen atom depends on to which neighbouring octahedra this atom belongs. If the neighbouring octahedra are different, the oxygen atom oscillates in a double-well potential as in $BaBiO_3$. If the octahedra are equal, the oxygen atom oscillates in a single-parabolic potential as in $BaPbO_3$ (see figure 6). The statistical weights of these two cases depend on the potassium content x, and are $1-x$ and x, respectively. Here, the force constants of the two parabolas are assumed to be equal since their independent variation

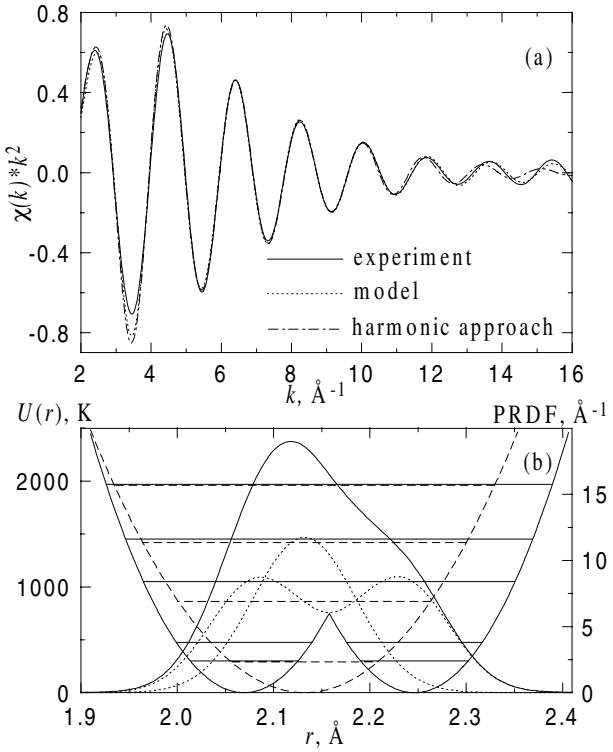

Figure 5. The experimental and model $\chi(k)k^2$ EXAFS for $Ba_{0.6}K_{0.4}BiO_3$ at 7 K for the first Bi–O near-neighbour shell (a) and the model potentials (single parabolic and double parabolic) with the corresponding PRDFs and energy levels (b). The total PRDF is shown by a solid line.

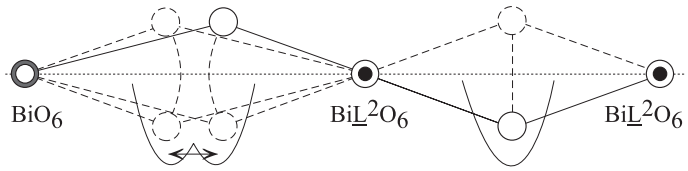

Figure 6. A sketch of the oxygen vibrations in $Ba_{1-x}K_xBiO_3$ in the case of different (left) and equivalent (right) neighbouring octahedra with corresponding radial oscillatory potentials.

does not improve the fits, and the number of fitting parameters equals 7. The resulting model curve is presented in figure 5(a) (dotted). It is seen from figure 5(b) that the total PRDF is unsplit, so it is not surprising that crystallographic measurements reveal the cubic structure [11] (e.g. at $T = 10$ K, $a = 4.2742(1)$). Meanwhile, the first momentum of the radial distribution function derived from our model is in good agreement with the diffraction data [11], which validates our calculated amplitudes and phases.

In this paragraph we address the important question of the statistical grounds for the choice among several possible models. Consider, first, the statistical chi-squared function (labelled just like the EXAFS function, but this is a different value)

$$\chi^2 = \frac{N_{exp}}{M}\sum_i^M \left(\frac{\chi_{exp}(k_i) - \chi_{mod}(k_i)}{\varepsilon_i}\right)^2 \tag{3}$$

where M is the number of data points in the fit, N_{exp} was introduced above, ε_i are the individual errors in the experimental data points. The latter were calculated as averages of $\sqrt{1/I_0 + 1/I_t}$, I_0 and I_t being the intensities measured in the transmission EXAFS experiment. The χ^2-value must follow the χ^2-distribution law with degrees of freedom $\nu = N_{exp} - P$, where P is the number of parameters varied during the fit. That is, χ^2 must be less than the critical value X^c_ν of the χ^2-distribution with ν degrees of freedom and the confidence level c. For our model in figure 5(a), $\nu_2 = 11 - 7 = 4$ and $\chi^2_2 = 5.3 < X^{0.95}_4 = 9.5$, but for a single-Gaussian model, $\nu_1 = 11 - 4 = 7$ and $\chi^2_1 = 16.8 > X^{0.95}_7 = 14.1$. Thus, our model passes the χ^2-test while the simple harmonic model does not. It is quite natural that, having increased the number of parameters, we got a decreased χ^2-value. But what should the gain be? The comparison between the two models can be performed on the basis of an F-test. If the difference $\chi^2_1 - \chi^2_2$ is physically meaningful, and not due to the presence of the noise—that is, if the simpler model cannot describe some features in principle—this difference must *not* follow the χ^2-distribution law with $\nu_1 - \nu_2$ degrees of freedom. Provided that χ^2_2 follows the χ^2-distribution with ν_2 degrees of freedom, the value

$$F(\nu_1 - \nu_2, \nu_2) = (\chi^2_1/\chi^2_2 - 1)\nu_2/(\nu_1 - \nu_2)$$

must not follow Fisher's F-distribution with $\nu_1 - \nu_2$ and ν_2 degrees of freedom. That is, F must be greater than the critical value $F^c_{\nu_1-\nu_2,\nu_2}$ of the F-distribution with $\nu_1 - \nu_2$ and ν_2 degrees of freedom and the confidence level c. Comparing the two models in figure 5(a), we find $F(3, 4) = 2.89$, which is equal to $F^{0.84}_{3,4}$. Therefore, we can claim with 84% probability that we propose a better model than the simplest single-Gaussian one.

The complete results for the Bi(Pb) octahedral ($N = 6$) oxygen environment in $BaPbO_3$ and $Ba_{1-x}K_xBiO_3$ with $x = 0$, 0.4, 0.5 at various temperatures are listed in table 1. The uncertainties in the EXAFS distances and force constants are less than $\pm 0.4\%$ and $\pm 50\%$, respectively. (These increments cause an increase of less than 10% in the value of the misfit.) It is seen from figures 3 and 5 that, in general, the positions of potential minima are not equal to the positions of PRDF maxima. Because of that, among other parameters, we give the values of PRDF centres of gravity, i.e. values that can be defined crystallographically. For $BaBiO_3$, the centres of gravity were calculated for the two peaks of PRDF separately.

The parameters of the potentials were obtained through the fit and, of course, depend on the form of the model potentials. To elucidate this influence, we constructed the model EXAFS function, using a polynomial of degree four:

$$U = -\kappa(r - r_0)^2/2 + \xi(r - r_0)^4 + \kappa^2/(16\xi)$$

where the last term is introduced to zero the minimum values (figure 7). The number of fitting parameters here is the same as for the double-parabolic potential. It turned out that for the two potential forms the mean frequencies of the Bi–O oscillations are practically identical for all temperatures. Because of this, in the present work we use double-parabolic potentials with parameters of clear meaning (potential minima positions and force constants) rather than a polynomial potential with abstract coefficients. Since the model EXAFS function weakly depends on the shape and value of the interwell energy barrier U_0, we cannot determine the U_0-value from the EXAFS measurements exactly.

It worth noticing that in the case of $BaBiO_3$ the above model of oxygen vibrations has some limitation due to the existence of the static rotation (tilting) distortion $\sim 11^\circ$. Thus, the distances observed from the EXAFS-spectra treatment are measured along the Bi–O–Bi zigzag curve, but not along the Bi–Bi ([100]) direction as in BKBO. This may result in some difference between the κ_1- and κ_2-values (see figure 3(b) and table 1) and some deviation of calculated frequencies from real ones for $BaBiO_3$.

Table 1. Bi(Pb)–O parameters resulting from the fit to EXAFS data for $BaPbO_3$ and $Ba_{1-x}K_xBiO_3$ with $x = 0$, 0.4, 0.5. r and l are positions (Å) of potential minima and corresponding PRDF first momenta; κ is the force constant (eV Å^{-2}). The index 0 corresponds to parabolic potentials; the indices 1 and 2 correspond to the two parts of the double-parabolic potentials.

	$BaPbO_3$		$x = 0$						$x = 0.4$					
T (K)	$r_0 = l$	κ_0	r_1	r_2	l_1	l_2	κ_1	κ_2	r_1	r_2	r_0	l	$\kappa_{1,2}$	κ_0
7	2.15	24	2.08	2.30	2.09	2.285	11	9	2.07	2.245	2.13	2.145	17	9
10	2.15	17												
20	2.155	15							2.07	2.235	2.13	2.14	28	18
30			2.09	2.305	2.095	2.295	15	14						
40	2.145	11							2.07	2.24	2.12	2.145	28	18
55			2.09	2.30	2.10	2.29	16	14	2.075	2.25	2.12	2.15	20	12
65			2.105	2.315	2.11	2.305	16	13	2.08	2.24	2.13	2.145	20	9
95	2.14	13	2.10	2.31	2.11	2.30	12	7						
115			2.10	2.31	2.11	2.30	11	6	2.08	2.24	2.12	2.14	18	10
135			2.105	2.31	2.11	2.30	13	5						
195									2.08	2.24	2.12	2.145	20	11
300	2.14	9	2.10	2.26	2.11	2.25	11	7	2.07	2.23	2.115	2.135	18	9

	$BaPbO_3$		$x = 0.5$					
T (K)	$r_0 = l$	κ_0	r_1	r_2	r_0	l	$\kappa_{1,2}$	κ_0
7	2.15	24	2.065	2.20	2.11	2.12	38	20
10	2.15	17	2.07	2.20	2.12	2.125	27	11
20	2.155	15	2.05	2.20	2.12	2.125	36	16
30			2.06	2.195	2.12	2.125	33	17
40	2.145	11						
55			2.07	2.20	2.12	2.125	41	22
65			2.06	2.20	2.12	2.125	39	21
95	2.14	13	2.06	2.20	2.125	2.13	32	17
115								
135			2.07	2.20	2.12	2.125	33	16
195								
300	2.14	9	2.07	2.205	2.125	2.13	24	11

4. The relationship between the local crystal and local electronic structures

4.1. $BaBiO_3$

The coexistence in $BaBiO_3$ of two different types of octahedron with two different Bi–O bond lengths and strengths reflects the different electronic structures of BiO_6 complexes.

Octahedral complexes represent the most tightly bound entities of the perovskite-like structures because of the strong covalence of the Bi 6s–O $2p_\sigma$ bonds. The valence band structure of $BaBiO_3$ is determined by the overlapping of Bi 6s and O 2p orbitals [1, 12], and, owing to strong Bi 6s–O $2p_\sigma$ hybridization, the octahedra can be considered as quasi-molecular complexes [35]. Each complex has ten electron levels consisting of a pair of bonding Bi 6s–O $2p_\sigma$ orbitals, six non-bonding O $2p_\pi$ orbitals, and a pair of antibonding Bi 6s–O $2p_{\sigma^*}$ orbitals. A unit cell, which includes two octahedra, has 38 valence electrons (10 from two bismuth ions, 4 from two barium ions, and 24 from six oxygen atoms). However, the numbers of occupied states in the two octahedral complexes are different: octahedron $Bi\underline{L}^2O_6$ carries 18 electrons and has one free level or a hole pair $\underline{L}^2$ in the upper antibonding Bi 6s–O $2p_{\sigma^*}$ orbital; in

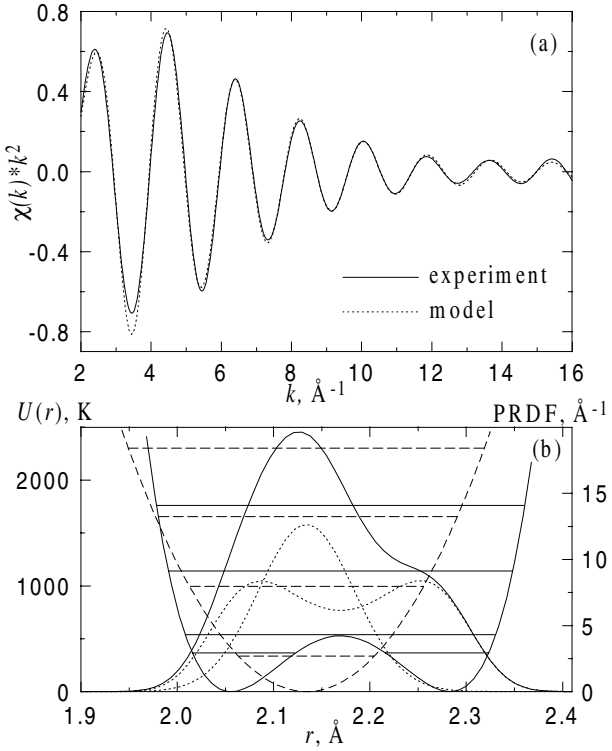

Figure 7. The experimental and model $\chi(k)k^2$ EXAFS for $Ba_{0.6}K_{0.4}BiO_3$ at 7 K for the first Bi–O near-neighbour shell (a) and the model potentials (single parabolic and polynomial of degree 4) with the corresponding PRDFs and energy levels (b). The total PRDF is shown by the solid line.

octahedron BiO_6 with 20 electrons both antibonding orbitals are filled (figure 8). It is quite natural that $Bi\underline{L}^2O_6$ octahedra have stiff (quasi-molecular) Bi–O bonds and the smaller radius, and BiO_6 octahedra represent non-stable molecules with filled antibonding orbitals and the larger radius. Because the sum of two nearest octahedra radii exceeds the lattice parameter a, the octahedral system must tilt around the [110] axis, producing a monoclinic distortion in $BaBiO_3$ (see figure 2).

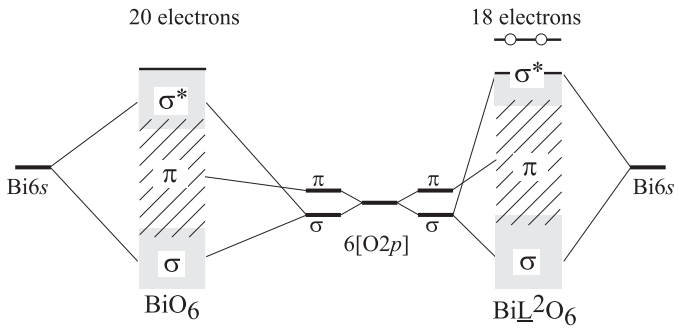

Figure 8. The scheme of electronic structure formation for two different octahedral BiO_6 complexes.

The assumption of equal electron filling for nearest octahedra ($Bi\underline{L}^1O_6$ + $Bi\underline{L}^1O_6$) contradicts experimental findings, since in this case equal Bi–O bond lengths and local magnetic ordering should be observed.

Therefore our new scheme of bismuth disproportionation $2Bi\underline{L}^1O_6 \rightarrow Bi\underline{L}^2O_6 + BiO_6$ is in full agreement with charge balance, the presence of two types of octahedron complex, and the absence of any local magnetic moment [36, 37].

Because Ba^{2+} in a perovskite-type lattice is bound by a pure ionic bond, the electron density is concentrated mainly in the octahedra volume V_0 [38]. Hence, the energy of the highest occupied level E_f is related to the octahedron radius R and the number of valence electrons N in a unit cell as

$$E_f \sim h^2 N^{2/3}/m_e V_0^{2/3} \sim h^2 N^{2/3}/m_e R^2 \tag{4}$$

where h is Planck's constant, m_e is the electron mass. This qualitative relation leaves out of account the deviation of the Fermi surface from a sphere [17]. Nevertheless, the value of E_f, which transforms to the Fermi level E_F for spatial overlapping of equal octahedra in the crystal, is in close connection with the octahedron radius and with the number of valence electrons.

According to expression (4), the local electronic structure is connected with the local crystal structure. On the left of figure 9(a), the case of the hypothetical simple cubic structure of $BaBiO_3$ is shown. The real monoclinic structure arises from combined breathing (alternating octahedra with different radii R) and rotation distortions, which, according to (4), leads to the lowering of the energy E_f of the highest occupied Bi 6s–O $2p_{\sigma^*}$ orbital in the BiO_6 octahedron

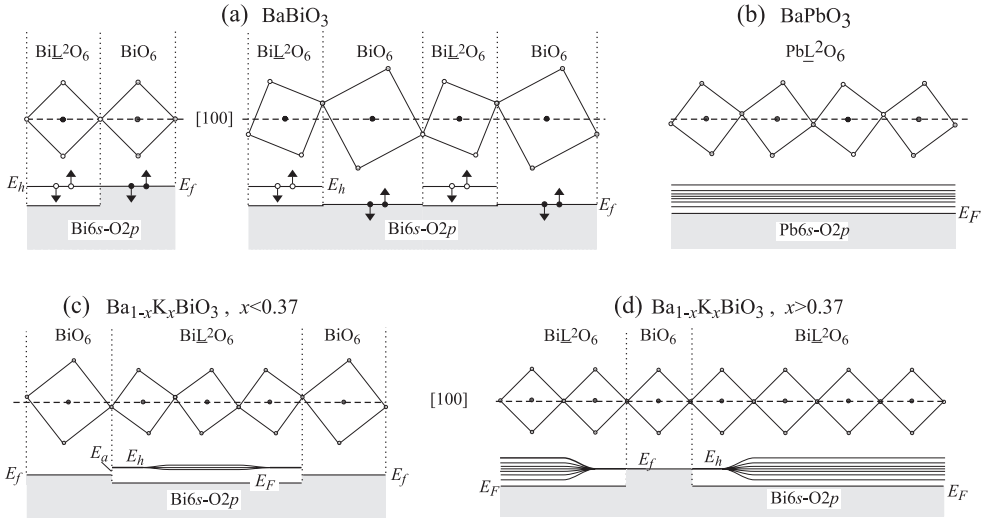

Figure 9. A schematic diagram of the relationship between the local crystal and local electronic structures. (a) The ground state of $BaBiO_3$. Left: in the cubic phase; right: in the monoclinic phase. E_h is the energy of the localized free level; E_f is the energy of the highest occupied Bi 6s–O $2p_{\sigma^*}$ orbital. The black and white circles with arrows denote electrons and holes, respectively, with opposite spin orientations. The occupied states of the Bi 6s–O 2p valence band are shown in grey. At the top, the local structure of the octahedral complexes is shown. The [100] direction is equivalent to the Bi–Bi direction. (b) The ground state of $BaPbO_3$. The unoccupied band above the Fermi level E_F is shown. (c) The ground state of $Ba_{1-x}K_xBiO_3$, $x < 0.37$. The splitting of the free level E_h when the spatial overlapping of $Bi\underline{L}^2O_6$ octahedra occurs is sketched. E_a is the activation energy $E_a = E_h - E_f$. (d) The ground state of $Ba_{1-x}K_xBiO_3$, $x > 0.37$. The formation of the unoccupied band above the Fermi level E_F when the percolation threshold is reached is sketched.

in comparison with the energy E_h of the unoccupied Bi 6s–O $2p_{\sigma^*}$ orbital in the $Bi\underline{L}^2O_6$ octahedron. Hence, the repetitive sequence of the empty levels E_h against the background of a fully filled valence band represents the electronic structure of the ground state of $BaBiO_3$ (figure 9(a), right). In such a system there are no free carriers and the conductivity occurs upon hopping of a carrier pair from one octahedron to another with the activation energy $E_a = E_h - E_f$. In this process the movement of a hole pair in real space leads to a change of large octahedra to small ones and vice versa or to a dynamic exchange $Bi\underline{L}^2O_6 \leftrightarrow BiO_6$, in full accordance with the vibrations in the double-well potential shown in figure 3, and causes hole-type conductivity. In this case, the activation energy E_a means the pair localization energy.

This picture agrees with the results of investigation of the temperature dependencies of the conductivity and Hall coefficient: $n(T) = n_0 \exp(-E'_a/k_BT)$ [17], where the value of the hole concentration $n_0 = 1.1 \times 10^{22}$ cm^{-3} coincides with the concentration of unit cells, and the activation energy $E'_a = 0.24$ eV, if one takes it into account that in the case of two-particle activation conductivity, the number of hole pairs is equal to the number of $Bi\underline{L}^2O_6$ complexes (the concentration of which is half n_0), and the activation energy $E_a = 2E'_a = 0.48$ eV. It should be mentioned that the possibility of the two-particle (bipolaron) conductivity being the most probable mechanism of conductivity in $BaBiO_3$ was pointed out earlier [17].

Pair splitting and hopping of a single electron from one octahedron to another costs energy and leads to electronic structure reconstruction of both octahedral complexes. Such a splitting can be achieved under optical excitation, which was observed experimentally as a photoconductivity peak at the photon energy $h\nu = 1.9$ eV [17]. The optical gap E_g is the energy difference between the excited and ground states. In the excited state, $BaBiO_3$ has the local lattice of equivalent octahedra $Bi\underline{L}^1O_6$ and possesses a non-compensated spin. Admittedly, it must have antiferromagnetic ordering, like the ground state in the undoped cuprates La_2CuO_4 and Nd_2CuO_4. Such optical excitation leads to the local dynamical lattice deformation observed in Raman spectra as a breathing mode $\sim$570 cm^{-1} of giant amplitude under resonant coincidence of the photon energy of an Ar^+ laser with E_g [35, 39, 40]. Using lasers with other quantum energies destroys this resonance effect and leads to an abrupt decrease of the breathing-mode amplitude [40].

Thus, the scheme proposed accounts for the nature of the two energy gaps in $BaBiO_3$. The activation energy E_a appears in transport measurements and is connected with coherent delocalization of hole pairs owing to the dynamic exchange $Bi\underline{L}^2O_6 \leftrightarrow BiO_6$. The optical gap is radically different from the traditional gap in semiconductors. It corresponds to the energy difference between the excited and ground states.

4.2. $BaPbO_3$

In $BaPbO_3$, each octahedron also has ten molecular orbitals, nine of which are filled, and one, antibonding Pb 6s–O $2p_{\sigma^*}$, which is unoccupied as in the octahedron $Bi\underline{L}^2O_6$, since lead has one electron fewer than bismuth. Thus, all the octahedral complexes represent the bound molecules $Pb\underline{L}^2O_6$ with equal radii. When spatial overlapping of $Pb\underline{L}^2O_6$ occurs in crystal $BaPbO_3$, the wave functions of the Pb 6s–O $2p_{\sigma^*}$ states become delocalized; unoccupied levels E_h of neighbouring octahedra split into a free-carrier band, and, merging with the top of the valence band consisting of initially filled Pb 6s–O $2p_{\sigma^*}$ orbitals, produce a half-filled conduction band (figure 9(b)). It is important to notice that unoccupied Bi(Pb) 6s–O $2p_{\sigma^*}$ orbitals in the case of the absence of spatial overlapping in $BaBiO_3$ behave as localized hole pairs, but transform to the conduction band when spatial overlapping occurs in $BaPbO_3$. Because of this, $BaBiO_3$ appears to be a semiconductor of p type, and $BaPbO_3$ appears to be a semimetal of n type.

Since the radius of the $Pb\underline{L}^2O_6$ complex is slightly greater than that of the $Bi\underline{L}^2O_6$ complex, the Fermi level E_F in $BaPbO_3$, according to expression (4), lies lower in comparison with E_f for $BaBiO_3$, which agrees with the results of photoelectron spectroscopy [41].

Thus, the lead valence state $Pb\underline{L}^2O_6$ in $BaPbO_3$ is similar to the bismuth state in $Bi\underline{L}^2O_6$ complexes in $BaBiO_3$. According to figure 4, oxygen atoms in $BaPbO_3$ oscillate in the parabolic potential without any exchange between equal $Pb\underline{L}^2O_6$ octahedra. Therefore, there is no charge-pair transfer in semimetallic $BaPbO_3$ and the itinerant electrons behave as the usual Fermi liquid.

4.3. $Ba_{1-x}K_xBiO_3$

The doping of $BaBiO_3$ by lead or potassium leads to a decrease of the integral structural lattice distortions and causes fundamental changes in both the local crystal and electronic systems. Firstly, we discuss the changes in the electronic structure of BKBO as a simpler case, and then we will extend the conclusions obtained to the BPBO system.

Since the K^+ ion has one valence electron rather than the two of the Ba^{2+} ion, the substitution of each set of two Ba^{2+} for two K^+ ions produces an additional unoccupied level or hole pair in a Bi 6s–O $2p_{\sigma^*}$ orbital and modifies the BiO_6 complex to $Bi\underline{L}^2O_6$. As a result, the ratio of the numbers of $Bi\underline{L}^2O_6$ and BiO_6 complexes changes from 1:1 in $BaBiO_3$ to $(1+x):(1-x)$ and equals 7:3 in $Ba_{0.6}K_{0.4}BiO_3$ and 3:1 in $Ba_{0.5}K_{0.5}BiO_3$. Spatial overlapping of $Bi\underline{L}^2O_6$ complexes occurs, which, taking into account their small radii and rigid bonds, contracts the lattice. This leads to the decrease and disappearance (at $x > 0.37$) of both static rotation-type and breathing-type distortions. The lattice is forced to contract, despite the ionic radii of Ba^{2+} and K^+ being practically equal.

Structural changes are accompanied by fundamental changes in the physical properties of BKBO: at $x \approx 0.37$ the insulator–metal phase transition occurs and the superconductivity that arises remains up to the dopant concentration $x = 0.5$ corresponding to the solubility limit of potassium in $BaBiO_3$. The type of the temperature dependence of the conductivity changes from semiconducting to metallic, the Hall coefficient changes its sign, and, in the normal state, the BKBO compound with $x > 0.37$ behaves as a metal with n-type conductivity [42].

These changes are well described in the framework of the above scheme (figure 9 for BKBO). At the low dopant level ($x < 0.37$), the contraction of the larger (soft) octahedron and the stretching of the smaller (rigid) octahedron, according to expression (4) bring the energies E_h and E_f close together, and the activation energy $E_a = E_h - E_f$ decreases. As dopant concentration rises, the number of $Bi\underline{L}^2O_6$ octahedra increases, and at $x > 0.37$, in the lattice there arise three-dimensional chains of spatially overlapping $Bi\underline{L}^2O_6$ octahedral complexes†; their unoccupied levels split and form the conductivity band, which is equivalent to the reaching of the percolation threshold that determines the insulator–metal phase transition. Here, the itinerant electrons show Fermi-liquid behaviour with the Fermi level E_F as in $BaPbO_3$. However, in contrast to the picture for $BaPbO_3$, in the BKBO structure there exist BiO_6 complexes through which itinerant electrons cannot move because all the levels in these complexes are occupied. The movement of electrons occupying the upper Bi 6s–O $2p_{\sigma^*}$ orbital is possible only in the pairing state when the dynamic exchange $Bi\underline{L}^2O_6 \leftrightarrow BiO_6$ occurs, since the unpairing costs energy. But, in contrast to the case for $BaBiO_3$, the static rotation- and breathing-type distortions of the octahedra disappear, their mean radii become approximately

† For the simple 3D case (levels 0 and 1 allowable, percolation through the cubic cell side) the percolation threshold is well known, $p_c \approx 0.31$. If the ground state represents the alternating cells of 0 and 1 states, our Monte Carlo calculations yield $p_c \approx 0.15$. If we additionally require that the percolating cluster must have at least one straight continuous chain in the chosen direction, the percolation threshold $p_c \approx 0.37$.

equal (and equal to half the lattice parameter), and the pair localization energy approaches zero: $E_a = E_h - E_f \rightarrow 0$ (figure 9(d)). In this case, the delocalized carrier pairs can move freely through the octahedral system which explains the appearance of superconductivity in BKBO ($x > 0.37$). This scheme of the local electronic structure is in full agreement with the picture of local oxygen vibration in a double-well potential (see figures 5, 6, 7).

The unpairing of electrons, as in $BaBiO_3$, is possible under optical excitation and is manifested by a pseudo-gap observed in reflectivity spectra even for the metallic phase of BPBO–BKBO systems. For instance, in BKBO with $x = 0.4$ the pseudo-gap is about 0.5 eV [43] and it is about 0.6 eV [17] in BPBO with $x = 0.25$.

The above model suggests that in the metallic phase two carrier types are present: itinerant electrons and pairs of initially (in $BaBiO_3$) localized carriers. The coexistence of the two carrier types was confirmed by experiments investigating the conductivity, Hall effect, and thermoelectric power [17], as well as by photoemission spectra [41, 44] and Raman spectra investigations [39, 45]. These results are in good agreement with the observed zero-bias conductance [46]. The change in carrier behaviour from localized to itinerant upon doping of $BaBiO_3$ by potassium was indicated by x-ray absorption spectra analysis at the O K absorption edge [21]. The analysis of EPR spectra [47, 48] showed the presence of the localized carrier pairs, which was also confirmed by the observation of two-particle tunnelling in the normal state of BKBO [46].

4.4. $BaPb_{1-x}Bi_xO_3$

Practically the same changes in electronic structure arise upon doping $BaBiO_3$ with lead. The electronic structure of the octahedral $Pb\underline{L}^2O_6$ complex is entirely equivalent to that of the $Bi\underline{L}^2O_6$ complex. Unoccupied levels of overlapping octahedra in $BaPbO_3$ form the conduction band, as when the overlapping of $Bi\underline{L}^2O_6$ in BKBO occurs. Upon doping $BaPbO_3$ with bismuth ($0 < x < 0.37$), the case is similar to that for BKBO ($x > 0.37$). However, in BPBO the following combinations of neighbouring octahedra are possible: $Pb\underline{L}^2O_6$–$Pb\underline{L}^2O_6$, $Pb\underline{L}^2O_6$–$Bi\underline{L}^2O_6$, $Pb\underline{L}^2O_6$–BiO_6, $Bi\underline{L}^2O_6$–BiO_6. This leads to different local shifts of the energies E_h and E_f, depending on different octahedra neighbouring pairs. With further increase of the bismuth content, the number of filled BiO_6 octahedra rises, the tilting and breathing distortions enlarge, the pair localization energy rises, and the spatial overlapping of unoccupied levels in $Pb\underline{L}^2O_6$ octahedra disappears, which destroys the metallic type of conductivity, and the system becomes a semiconductor with p-type conductivity.

Thus, superconductive properties of BPBO in our model are connected with dynamic exchange, $Pb\underline{L}^2O_6 \leftrightarrow BiO_6$. Unfortunately, it is practically impossible to observe the double-well-potential oxygen vibrations for superconducting BPBO compositions ($0 < x < 0.35$) by EXAFS study because of the overlapping of Pb L_3 and Bi L_3 edges. Though an analysis of EXAFS spectra for these compounds is possible with an elaborate treatment procedure [49], precise enough values can be obtained only for interatomic distances, and not for amplitude factors. For this reason, we do not present the EXAFS data for BPBO ($0 < x < 1$) in this paper.

4.5. Photoemission spectra anomalies

The analysis of photoemission spectra has revealed a serious contradiction concerning the experimental observation of the splitting of the Bi 4f(5/2, 7/2) spectral lines in superconducting BKBO compounds [50] in the absence of any peculiarities of those lines in the parent $BaBiO_3$ [44]. The contradiction consists in the feature that, though the analysis of x-ray diffraction

and EXAFS data indicates the existence of two different Bi–O bonds in $BaBiO_3$, no splitting of Bi 4f doublet lines was observed, which indicates the absence of considerable difference in bismuth valence states. The doping of $BaBiO_3$ by potassium relieves the monoclinic distortion and equalizes the Bi–O bond lengths up to $a/2$. However, the Bi 4f spectral lines become broadened [44] and, in measurements on a high-resolution spectrometer, even split [50], which, in contrast with a simple cubic lattice in BKBO ($x > 0.37$), indicates the existence of two different bismuth valence states.

The above scheme of local electronic structure completely resolves this issue. Indeed, in $BaBiO_3$ the binding energies of the Bi 4f core levels in different $Bi\underline{L}^2O_6$ and BiO_6 octahedra are almost equal, and, hence, the Bi 4f doublet lines in photoemission spectra are unsplit (figure 10(a)). Contrary to this, in $Ba_{0.6}K_{0.4}BiO_3$, the binding energies of the Bi 4f core levels in the different octahedra, E'_1, E'_2 and E_1, E_2, differ in $\Delta E = E_h - E_F \approx E_a$, which causes the broadening (see the curve for $x = 0.5$ in figure 10(a) from [44]) and splitting (see the curve for $x = 0.4$ in figure 10(b) from [50]) of the Bi 4f doublet lines. The value of the

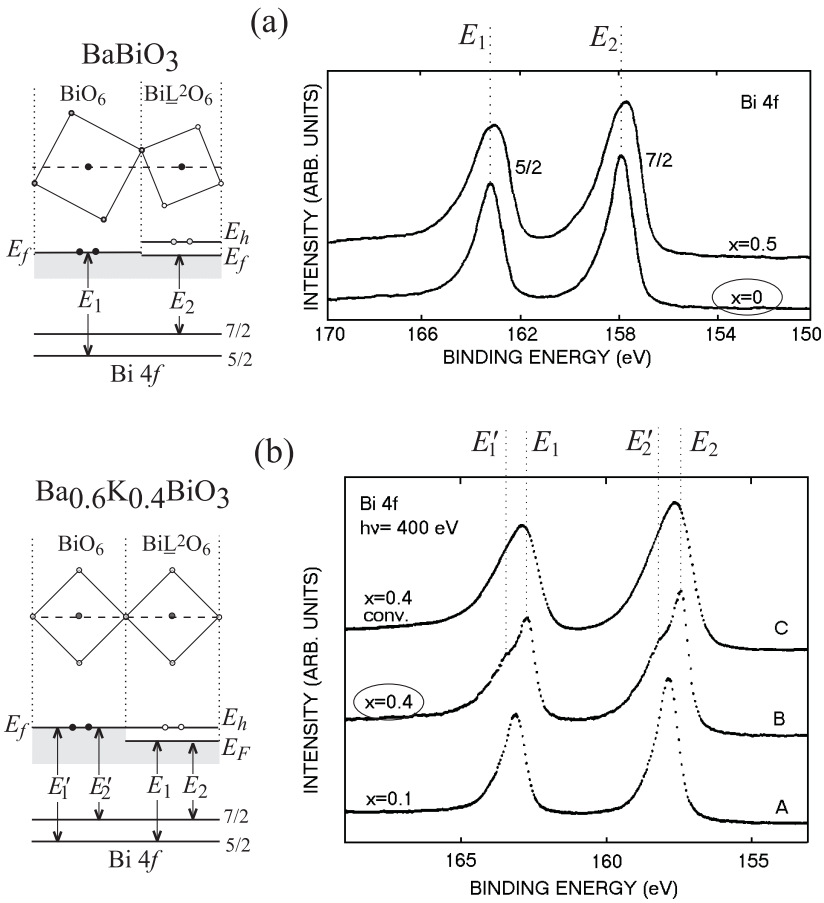

Figure 10. Binding energies of Bi 4f(5/2, 7/2) core levels in $Ba_{1-x}K_xBiO_3$: (a) for $x = 0$, right: experimental photoemission spectra from [44] with energy resolution $\Delta E = 0.45$ eV; (b) for $x = 0.4$, right: experimental photoemission spectra from [50] with energy resolution $\Delta E = 0.25$ eV. Curve C is the result of the convolution of curve B with a Gaussian function with 0.75 eV width.

splitting coincides well with our estimate of $E_a = 0.48$ eV, and the ratio of intensities I of the core-level peaks corresponding to the binding energies in different octahedral complexes BiO_6 and $Bi\underline{L}^2O_6$ is in accordance with the relative content of these complexes in $Ba_{0.6}K_{0.4}BiO_3$: $I(E_1')/I(E_1) \simeq I(E_2')/I(E_2) \simeq 3/7$.

5. On the possible nature of the superconducting state

The essentially anharmonic character of oxygen-ion oscillations in the soft rotation mode is the basis of the anharmonic model of high-temperature superconductivity [4]. It was shown that the anharmonic coupling constant λ_s exceeds the constant in the harmonic approach λ_{ph}:

$$\lambda_s/\lambda_{ph} \simeq J_s^2 d^2 \bar{\omega}/J_{ph}^2 \langle u^2 \rangle \omega_s \gg 1 \tag{5}$$

which explains the high critical temperatures in cuprate HTSC compounds as well as in BPBO–BKBO systems. Here, d and ω_s are the amplitude and frequency of oscillation in a double-well potential, $\langle u^2 \rangle$ is the mean square displacement of the ions with the mean frequency $\bar{\omega}$ in the harmonic approach, J_{ph}^2 and J_s^2 are, respectively, the deformation potentials of harmonic and anharmonic oscillations averaged on the Fermi surface.

In that model, the oscillatory movement of oxygen ions in the rotation mode with a large amplitude in the direction perpendicular to the Bi(Pb)–O bonds was considered. The considerable gain in value of the coupling constant in expression (5) is due to the low frequency of the soft rotation mode ($\omega_s < \bar{\omega}$) and the excess of its amplitude over the amplitude of the harmonic oscillations ($d^2 \gg \langle u^2 \rangle$).

Meanwhile, previous [12, 38, 51] as well as recent (see [52] and references therein) electronic structure calculations showed that such a movement hardly affects the Bi–O bond lengths, keeping the sp(σ) nearest-neighbour interaction nearly constant. Thus, despite the existence of the double-well potential in the rotation (tilting) mode, Meregalli and Savrasov [52] obtained a very small anharmonic contribution to λ. Also, they assumed the breathing-type oxygen vibrations to be harmonic with small amplitude and high frequency, and found too small a value of λ, $\approx$0.3, to explain the high T_c for BKBO.

Our investigation firstly showed that in BKBO the double-well vibrations with strong deformation potential also exist along the Bi–O–Bi direction. Such vibrations have the breathing-like character and low frequency bounded by a soft rotation mode. Thus, our results resolve the above issue and explain the reason for strong electron–phonon coupling in Bi-based oxides. Also, to these vibrations we can assign the low-frequency part, below 40 meV, of the phonon density of states observed in neutron scattering investigation for superconducting BKBO [53] and absent in calculations [52]. Also, the anomalous phonon softening along the [100] direction [54] becomes clear due to our observation of coherent breathing-like vibrations along the [100] axis.

Hardy and Flocken [5] evaluated values of λ, using abstract model double-well potentials:

$$\lambda(T) = N(0) \sum_{kk'}^{FS} \sum_{n'>n} \frac{|\langle n|M_{kk'}|n'\rangle|^2}{E_{n'} - E_n} (f_n - f_{n'}) \tag{6}$$

where $N(0)$ is the density of electron states at the Fermi level, $M_{kk'}$ is the electron–phonon matrix element connecting the electronic states $|k\rangle$ and $|k'\rangle$ on the Fermi surface, $|n\rangle$ and $|n'\rangle$ are the oscillatory states with energies E_n and $E_{n'}$, f_n and $f_{n'}$ are the thermal weighting factors:

$$f_n = \exp(-E_n/kT) \Big/ \sum_{n'} \exp(-E_{n'}/kT).$$

Given the oscillatory energies from our EXAFS experiment, we have calculated λ in terms of an arbitrary multiplicative constant which is proportional to $N(0)$ and $M_{kk'}$

(figure 11). Although the 'phonon' part of λ is the strongest for $BaBiO_3$, this composition is not superconducting: on the one hand, because of the pair localization energy E_a; on the other, because the rotation oscillations of rigid $Bi\underline{L}^2O_6$ octahedra and ordinary phonons (of stretching and bending types) differ in collective character of motion in BiO_2 planes. In $BaBiO_3$, rigid $Bi\underline{L}^2O_6$ octahedra are separated by soft BiO_6 octahedra and are not spatially overlapping. The partial replacement of the larger soft octahedra by the smaller rigid ones upon potassium doping leads to the decrease and disappearance of the localization energy E_a (figures 9(c), 9(d)) and to spatial coherence of rotation oscillations with the length of several lattice parameters, depending on the doping level x. For superconducting compositions, T_c means the temperature up to which λ is considerably decreased (figure 11) and/or the coherence in oscillations of neighbouring octahedra is thermally destroyed by ordinary phonons.

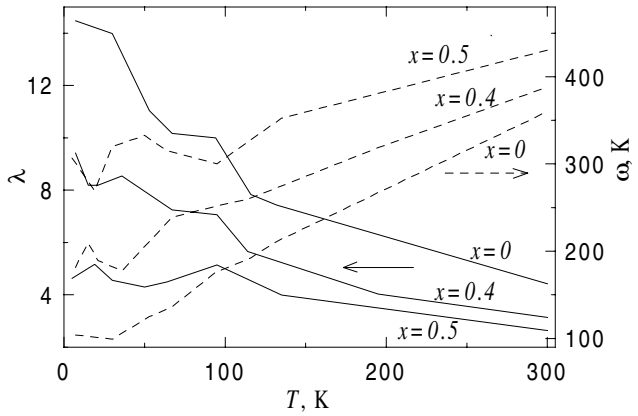

Figure 11. λs in terms of an arbitrary multiplicative constant (solid lines) and mean oscillatory frequencies (dashed lines) for $Ba_{1-x}K_xBiO_3$ with $x = 0$, 0.4, 0.5 for double-well potentials obtained from EXAFS-spectra treatment.

The above-described ground state of $BaBiO_3$ can be considered as a bipolaronic state as well, and the movement of carrier pairs correlated with oxygen-atom oscillation when the dynamic exchange $Bi\underline{L}^2O_6 \leftrightarrow BiO_6$ occurs is evidence for possible applicability of bipolaron theory [55], which is supported by the small size of the pair (size of an octahedron) and by the existence of the pair state above T_c.

6. Conclusions

From the EXAFS investigation of BPBO–BKBO systems, local crystal structure peculiarities connected with non-equivalence of $Bi\underline{L}^2O_6$–BiO_6 octahedra were observed. It was found that oxygen vibrations are well described using double-well potentials, which leads to the strong electron–phonon coupling due to coherent modulation of Bi–O bond lengths with low frequency and causes carrier-pair movement correlated with oxygen-ion oscillations. The underlying relationship between the local crystal and local electronic structures was established; it explains the full list of unusual properties of BPBO–BKBO systems: the existence of two energy gaps (transport E_a and optical E_g) in $BaBiO_3$; the mechanism of two-particle conductivity in $BaBiO_3$; the coexistence of two different carrier types; pseudo-gap observation for metallic compositions of BKBO and BPBO systems; the existence of zero-bias conductance; the observation of localized pairs from EPR spectra; the observation of low-frequency (<40 meV) phonons; the nature of the concentration and temperature

phase transitions; the contradictions between the findings from local (Raman and EXAFS) and integral structural methods for metallic BKBO; the anomalies of the XPS spectra for $BaBiO_3$ and BKBO. We observed the correlated movement of carrier pairs and low-frequency breathing-like oxygen octahedra vibrations, which corresponds to a superconducting state. The model proposed combines some principal features of the real-space pairing [56], anharmonic models [4, 5], and bipolaron theory [55] of high-T_c superconductivity.

The similarity of the rotation-mode peculiarities of BiO_6 octahedra and CuO_n complexes and the observed anomalies in temperature dependencies of Debye–Waller factors in cuprates [57] allow one to hope that a similar model approach could be applied to the copper-based superconductors.

Acknowledgments

We acknowledge the LURE Programme Committee for providing beamtime, and Professors S Benazeth and J Purans for help during the x-ray absorption measurements. We are also grateful to Professor A P Rusakov for high-quality BKBO samples and to Dr A V Kuznetsov and Dr A A Ivanov for helpful discussions. The work was supported by the Russian Foundation for Basic Research (Grant No 99-02-17343), and the Programmes 'Universities of Russia' (Grant No 4066) and 'Superconductivity' (Grant No 99010).

References

[1] Sleight A W, Gillson J L and Bierstedt P E 1973 *Solid State Commun.* **17** 27–8
[2] Plakida N M 1995 *High-Temperature Superconductivity* (Berlin: Springer)
[3] Wignacourt J P, Swinnea J S, Steinfink H and Goodenough J B 1988 *Appl. Phys. Lett.* **53** 1753–5
Kwei G H, Goldstone J A, Lawson A C Jr, Thompson J D and Williams A 1989 *Phys. Rev.* B **39** 7378–80
[4] Plakida N M, Aksenov V L and Drechsler S L 1987 *Europhys. Lett.* **4** 1309–18
[5] Hardy J R and Flocken J W 1988 *Phys. Rev. Lett.* **60** 2191–3
[6] Mattheiss L F, Gyogry E M and Jonson D W Jr 1988 *Phys. Rev.* B **37** 3745–6
[7] Stepankin V N, Protasov E A, Kuznetsov A V and Zaitsev-Zotov S V 1985 *Pis. Zh. Eksp. Teor. Fiz.* **41** 23–6 (Engl. Transl. 1985 *JETP Lett.* **41** 27–30)
[8] Schlesinger Z, Collins R T, Calise J A, Hinks D G, Mitchel A W, Zheng Y, Dabrowski B, Bickers N E and Scalapino D J 1989 *Phys. Rev.* B **40** 6862–6
[9] Allen P B 1988 *Nature* **335** 396–7
[10] Marx D T, Radaelli P G, Jorgensen J D, Hitterman R L, Hinks D G, Pei S and Dabrowski B 1992 *Phys. Rev.* B **46** 1144–56
[11] Pei S, Jorgensen J D, Dabrowski B, Hinks D G, Richards D R, Mitchell A W, Newsam J M, Sinha S K, Vaknin D and Jacobson A J 1990 *Phys. Rev.* B **41** 4126–41
[12] Mattheiss L F and Hamann D R 1983 *Phys. Rev.* B **28** 4227–41
[13] Cox D E and Sleight A W 1989 *Acta Crystallogr.* B **35** 1–10
[14] Wertheim G K, Remeika J P and Buchanan D N E 1982 *Phys. Rev.* B **26** 2120–3
[15] Akhtar Z N, Akhtar M J and Catlow C R A 1993 *J. Phys.: Condens. Matter* **5** 2643–6
[16] Hashimoto T, Kawazoe H and Shimamura H 1994 *Physica* C **223** 131–9
[17] Uchida S, Kitazawa K and Tanaka S 1987 *Phase Transitions* **8** 95–128
[18] Yacoby Y, Heald S M and Stern E A 1997 *Solid State Commun.* **101** 801–6
[19] Anshukova N V, Golovashkin A I, Gorelik V S, Ivanova L I and Rusakov A P 1990 *J. Mol. Struct.* **219** 147–151
[20] Heald S M, Di Marzio D, Croft M, Hegde M S, Li S and Greenblatt M 1989 *Phys. Rev.* B **40** 8828–33
[21] Salem-Sugui Jr S, Alp E E, Mini S M, Ramanathan M, Campuzano J C, Jennings G, Faiz M, Pei S, Dabrowski B, Zheng Y, Richards D R and Hinks D G 1991 *Phys. Rev.* B **43** 5511–5
[22] Boyce J B, Bridges F G, Claeson T, Geballe T H and Remeika J M 1990 *Phys. Rev.* B **41** 6306–14
[23] Menushenkov A P, Benazeth S, Purans J, Ignatov A Yu and Klementev K V 1997 *Physica* C **277** 257–64
[24] Koyama Y, Nakamura S I and Inoue Y 1992 *Phys. Rev.* B **46** 9186–9
[25] Menushenkov A P 1996 *Proc. Int. Workshop on High Temperature Superconductivity—Ten Years after its Discovery* ed K B Karg and S M Bose (Jaipur: Narosa) p 155

Menushenkov A P 1998 *Nucl. Instrum. Methods* A **405** 365–9
[26] Mustre de Leon J, Conradson S D, Batistić I, Bishop A R, Raistrick I D, Aronson M C and Garzon F H 1992 *Phys. Rev.* B **45** 2447–57
[27] Klementev K V 1998 *XAFS-X: Int. Conf. on X-ray Absorption Fine Structure (Chicago, IL, 10–14 Aug 1998)* abstracts p 132 (T5.2-14)
The program is freely accessible from
http://www.crosswinds.net/~klmn/viper.html
[28] Ignatov A Yu, Menushenkov A P and Chernov V A 1996 *Physica* C **271** 32–50
[29] Anshukova N V, Golovashkin A I, Ivanova L I, Malyuchkov O T and Rusakov A P 1995 *IEEE Trans. Magn.* 1325–7
[30] Newville M, Līviņš P, Yacoby Y, Rehr J J and Stern E A 1993 *Phys. Rev.* B **47** 14 126–31
[31] Stern E A 1993 *Phys. Rev.* B **48** 9825–7
[32] Rehr J J, Mustre de Leon J, Zabinsky S I and Albers R C 1991 *J. Am. Chem. Soc.* **113** 5135–40
[33] Balzarotti A, Menushenkov A P, Motta N and Purans J 1984 *Solid State Commun.* **49** 887–90
[34] Boyce J B, Bridges F G and Claeson T 1992 *Phys. Scr.* **42** 71–5
[35] Sugai S 1987 *Japan. J. Appl. Phys. Suppl.* 3 **26** 1123–4
[36] Uchida S, Hasegawa H, Kitazawa K and Tanaka S 1988 *Physica* C **156** 157–64
[37] Uemura Y J, Sternlieb B J, Cox D E, Kadono R, Brewer J H, Kempton J R, Kiefl R F, Kreitzman S R, Luke J M, Mulhern P, Riseman T, Williams D L, Kossler W J, Yu X H, Stronach C E, Subramanian M A, Gopalakrishnan J and Sleight A W 1988 *Nature* **335** 151–2
[38] Hamada N, Massidda S, Freeman A J and Redinger J 1989 *Phys. Rev.* B **40** 4442–52
[39] Sugai S, Uchida S, Kitazawa K, Tanaka S and Katsui A 1985 *Phys. Rev. Lett.* **55** 426–9
[40] Tajima S, Yoshida M, Koshizuka N, Sato H and Uchida S 1992 *Phys. Rev.* B **46** 1232–5
[41] Namatame H, Fujimori A, Torii H, Uchida T, Nagata Y and Akimitsu J 1994 *Phys. Rev.* B **50** 13 674–8
[42] Sato H, Ido T, Ushida S, Tajima S, Yoshida M, Tanabe K, Tatsubara K and Miura N 1993 *Phys. Rev.* B **48** 6617–25
[43] Blanton S H, Collins R T, Kelleher K H, Rotter L D, Schlesinger Z, Hinks D G and Zheng Y 1993 *Phys. Rev.* B **47** 996–1001
[44] Nagoshi M, Suzuki T, Fukuda Y, Ueki K, Tokiwa A, Kikuchi M, Syono Y and Tachiki M 1992 *J. Phys.: Condens. Matter* **4** 5769–81
[45] Sugai S 1987 *Phys. Rev.* B **47** 3621–4
[46] Hellman E S and Hartford E H Jr 1995 *Phys. Rev.* B **52** 6822–8
[47] Misra S K, Andronenko S I, Andronenko R R and Mezentseva L P 1996 *Phys. Rev.* B **53** 9442–7
[48] Yakubovskii A, Gudenko S, Rusakov A, Golovashkin A and Verhovskii S 1997 *Physica* C **282–287** 1929–30
[49] Boyce J B, Bridges F G, Claeson T, Geballe T H, Li G G and Sleight A W 1991 *Phys. Rev.* B **44** 6961–7
[50] Qvarford M, Nazin V G, Zakharov A A, Mikheeva M N, Anderson J N, Johansson M K J, Rogelet T, Söderholm S, Tjernberg O, Nylén H, Lindau I, Nyholm R, Karlsson U O, Barilo S N and Shiryaev S V 1996 *Phys. Rev.* B **54** 6700–7
[51] Shirai M, Suzuki N and Motizuki K 1990 *J. Phys.: Condens. Matter* **2** 3553–66
[52] Meregalli V and Savrasov S Y 1998 *Phys. Rev.* B **57** 14 453–69
[53] Loong C-K, Vashishta P, Kalia R K, Jin W, Degani M H, Hinks D G, Price D L, Jorgensen J D, Dabrowski B, Mitchell A W, Richards D R and Zheng Y 1992 *Phys. Rev.* B **45** 8052–64
[54] Braden M, Reichardt W, Schmidbauer W, Ivanov A S and Rumiantsev A Yu 1995 *J. Supercond.* **8** 595–8
[55] Alexandrov A S and Ranninger J 1989 *Phys. Rev.* B **23** 1796–801
Alexandrov A S 1981 *Physica* C **158** 337–44
[56] Rice T M and Sneddon L 1981 *Phys. Rev. Lett.* **47** 689–92
[57] Maruyama H, Kimura H, Koizumu A, Yamazaki H, Maeda H and Ishii T 1991 *X-Ray Absorption Fine Structure* ed S S Hasnain (New York: Ellis Horwood) p 370
Yamaguchi H, Oyanagi H, Ihara H, Kuwahara Y and Syono Y 1991 *X-Ray Absorption Fine Structure* ed S S Hasnain (New York: Ellis Horwood) p 380